Spectroscopy of Na_2 Using Laser-Induced Fluorescence*

W. DEMTRÖDER†
Joint Institute for Laboratory Astrophysics, University of Colorado, Boulder, Colorado 80302
AND
M. MCCLINTOCK
National Bureau of Standards and Department of Physics and Astrophysics, University of Colorado, Boulder, Colorado 80302
AND
R. N. ZARE‡
Joint Institute for Laboratory Astrophysics and National Bureau of Standards, Boulder, Colorado 80302

(Received 18 April 1969)

The argon-ion laser lines at 4658, 4727, 4765, 4880, 4965, 5017, and 5145 Å are each found to excite one or more resonance fluorescence series of the Na_2 ($X\ ^1\Sigma_g^+$–$B\ ^1\Pi_u$) blue-green band system. Altogether, 19 different fluorescence progressions have been identified and assigned v, J quantum numbers. The absolute wavenumbers of many of these emission lines have been measured interferometrically using a Fabry–Perot etalon crossed with a Bass–Kessler type spectrograph. A revised set of spectroscopic constants has been determined for both the upper and lower states which reproduce the observed term energies to better than 0.1 cm^{-1} on the average. Using these improved spectroscopic data, potential curves have been constructed for the B and X states of Na_2 by the Rydberg–Klein–Rees method. These potential curves are used in turn to compute Franck–Condon factors for the Na_2 B–X band system.

I. INTRODUCTION

Laser-induced fluorescence of molecules[1,2] is a recent development which gives promise not only of permitting detailed spectroscopic studies of molecular structure, but also of serving as an excellent means of preparing a significant number of molecules in a known vibrational–rotational quantum state so that we may observe the subsequent energy transfer processes they undergo. We report here the accurate determination of spectroscopic constants, potential curves, and Franck–Condon factors for the Na_2 ($X\ ^1\Sigma_g^+$–$B\ ^1\Pi_u$) blue-green band system based on the interferometric analysis of 19 different fluorescence series excited in the Na_2 molecule by the cw lines of the argon-ion laser.

When an alkali metal in an evacuated container is warmed a few hundred degrees above its melting point, the vapor contains about 1% or less of alkali dimer molecules.[3] At first thought these trace species might seem to be of little interest. However, a brief review of past investigations of alkali dimer molecules shows that their study has been responsible for many contributions to our basic understanding of molecular structure.

The first spectroscopic studies of alkali dimers appear to have been the work of Wiedemann and Schmidt in 1891.[4] They irradiated a vessel of sodium vapor with the focussed rays of the sun and observed, in addition to the bright sodium D lines, an intense yellowish-green fluorescence which seemed to have light and dark bands when viewed through a small spectroscope. The spectrum of the emission was first photographed in 1903 by Wood and Moore[5] and appeared to be nearly complementary to the absorption spectrum. An extensive study of this phenomenon, undertaken by Wood,[6] led to the discovery of resonance fluorescence. A monochromator was placed in front of the arc source that was used to illuminate the sodium vapor. By narrowing the slits of this monochromator so that the transmitted light was not much greater in width than one of the sodium absorption lines, Wood reports: "It was at once apparent that the character of the spectrum was much altered, and as the wavelength of the exciting light was slowly changed, the lines of the fluorescent

* This cooperative project was supported by National Science Foundation Grant GP-8095, National Institute of Health Grant GM 11123-04, and by the Advanced Research Projects Agency of the Department of Defense monitored by Army Research Office—Durham under Contract DA-31-124-ARO-D-139.

† JILA Visting Fellow, 1967–1968. Present address: Physikalisches Institut der Universität, Freiburg, Germany.

‡ Alfred P. Sloan Fellow. Present address: Chemistry Department, Columbia University, New York.

[1] For laser-induced infrared fluorescence of gas-phase molecules see (a) L. O. Hocker, M. A. Kovacs, C. K. Rhodes, G. W. Flynn, and A. Javan, Phys. Rev. Letters **17**, 233 (1966); M. Kovacs, D. Ramachandra Rao, and A. Javan, J. Chem. Phys. **48**, 3339 (1968). (b) J. T. Yardley and C. B. Moore, *ibid.* **45**, 1066 (1967); C. B. Moore, R. E. Wood, B. Hu, and J. T. Yardley, *ibid.* **45**, 4222 (1967); J. T. Yardley and C. B. Moore, *ibid.* **48**, 14 (1968); J. C. Stephenson, R. E. Wood, and C. B. Moore, *ibid.* **48**, 4790 (1968). (c) M. C. Bordé, A. Henry, and M. L. Henry, Compt. Rend. **B262**, 1389 (1966); **B263**, 619 (1967). (d) A. M. Ronn, J. Chem. Phys. **48**, 511 (1968).

[2] For laser-induced electronic (visible) fluorescence of gas-phase molecules see (a) W. J. Tango, J. K. Link, and R. N. Zare, Bull. Am. Phys. Soc. **12**, 1147 (1967); **13**, 847 (1968); J. Chem. Phys. **49**, 4264 (1968). (b) S. Ezekiel and R. Weiss, Phys. Rev. Letters **20**, 91 (1968); J. I. Steinfeld, J. D. Campbell, and N. A. Weiss, J. Mol. Spectry. **29**, 204 (1969); K. Sakurai and H. P. Broida, J. Chem. Phys. **50**, 557 (1969). (c) M. McClintock and L. C. Balling, Bull. Am. Phys. Soc. **13**, 55 (1968); "Molecular Fluorescence from Laser-Excited Diatomic Cesium and Rubidium," J. Quant. Spectry. Radiative Transfer (to be published).

[3] M. Lapp and L. P. Harris, J. Quant. Spectry. Radiative Transfer **6**, 169 (1966); A. N. Nesmeyanov, *Vapour Pressure of the Elements* (Academic Press Inc., New York, 1963).

[4] E. Wiedemann and G. C. Schmidt, Ann. Physik **42**, 448 (1891); **57**, 447 (1896).

[5] R. W. Wood and J. H. Moore, Astrophys. J. **18**, 94 (1903).

[6] R. W. Wood, Phil. Mag. **10**, 513, 521 (1905); **12**, 499 (1906); **15**, 581 (1908); **16**, 184 (1908); **18**, 530 (1909); **26**, 846 (1913); **27**, 1025 (1914); R. W. Wood and E. L. Kinsay, Phys. Rev. **30**, 1 (1927); **31**, 793 (1928).

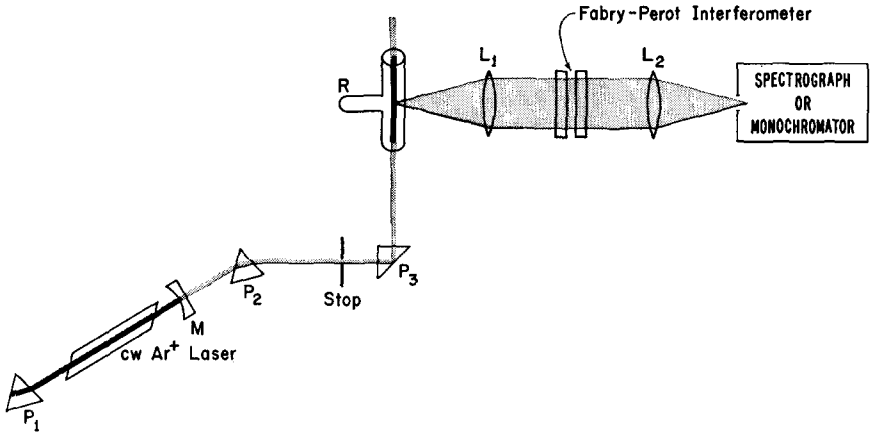

FIG. 1. Experimental setup for laser-induced fluorescence spectroscopy. Here M=mirror, L=lens, P=prism and R=reservoir.

spectrum appeared to move about in the liveliest manner. The whole spectrum appeared in motion, the luminous bands moving in a rippling manner, like moonlight on water."[7] Photographs of the emission showed that a series of bright narrow lines of nearly equidistant spacing was produced for each setting of the monochromator's wavelength. From these observations, Wood was led to replace the light from the monochromator with the sharp atomic emission lines obtained from a metallic arc. In this way, he found more than 15 different atomic lines which caused what we now call a resonance fluorescence progression, or a Wood's series.

All these bands and series were first ascribed to atomic sodium. However, in a book published in 1921, which helped to lay the foundation of our present-day understanding of fluorescence and phosphorescence, Pringsheim[8] suggested that the Na_2 molecules were the carriers of the fluorescence. When an atomic line overlaps a molecular absorption line, the molecule is excited to a particular vibrational–rotational level of the upper electronic state. From this excited level the molecule emits a series of lines corresponding to those possible transitions terminating on all the vibrational–rotational levels of the ground state which satisfy the rotational selection rules appropriate to the molecular band system. The Franck–Condon principle governs the vibrational intensity distribution. Subsequent investigations of the absorption and emission spectra of the alkali dimers have provided, for example, (1) evidence for and the value of the nuclear spin of the alkali atoms based on the intensity alternation of the rotational lines in absorption,[9] (2) confirmation of the essential correctness of the Franck–Condon principle from the agreement between the calculated and observed intensity pattern of the Na_2 resonance fluorescence progressions,[10] (3) proof for the existence of perturbations in molecular spectra from magnetic rotation studies,[11] and (4) evidence that the potential curves of certain alkali dimer excited states have bumps in them as they approach the dissociation limit.[12] The fact that so many of these discoveries are now regarded as common knowledge indicates the debt we owe to the early investigators of the alkali dimer molecules.

In recent years there has been increasing interest in precise knowledge of molecular constants, Franck–Condon factors, and potential curves of alkali diatomic molecules. This has been stimulated in part by the numerous theoretical calculations of the electronic structure of these molecules.[13] At first it might appear that the alkali dimers would closely resemble the hydrogen molecule; the electrons could be partitioned into atomic core electrons which shield the charge of the nucleus and two valence electrons which are responsible for the molecular binding. However, recent experiments[14] have demonstrated that the alkali dimer ions are more stable than their neutral dimer parents, whereas it is well known that H_2 is more tightly bound than H_2^+. Accordingly, accurate measurements of the form of the molecular potential curves and the value of the molecular constants will be a useful check on the validity of any theoretical calculations which attempt to explain the nature of chemical binding in these seemingly simple molecules.

Another reason motivating the study of the struc-

[7] R. W. Wood, *Physical Optics* (The MacMillan Co., New York, 1934), p. 621. The frontispiece of this book magnificently illustrates in color several Na_2 resonance fluorescence series which Wood found using arc-line excitation.

[8] P. Pringsheim, *Fluorescenz und Phosphorescenz im Lichte der neueren Atomtheorie* (Springer-Verlag, Berlin, 1921).

[9] H. C. Urey, Phys. Rev. **38**, 1074 (1931); F. W. Loomis, *ibid.* **38**, 2153 (1931).

[10] W. G. Brown, Z. Physik **82**, 768 (1933).

[11] W. R. Fredrickson and C. R. Stannard, Phys. Rev. **44**, 632 (1933); T. Carroll, *ibid.* **52**, 822 (1937).

[12] See G. W. King and J. H. Van Vleck, Phys. Rev. **55**, 1165 (1939).

[13] For the Na_2 molecule see, for example, (a) G. Das, J. Chem. Phys. **44**, 87 (1966); **46**, 1568 (1967). (b) L. Szasz and G. McGinn, J. Chem. Phys. **45**, 2898 (1966); **48**, 2997 (1968). (c) P. J. Bertonicini, G. Das, and A. C. Wahl, Bull. Am. Phys. Soc. **13**, 81 (1968).

[14] R. F. Barrow, N. Travis, and C. V. Wright, Nature **187**, 141 (1960). E. W. Robertson and R. F. Barrow, Proc. Chem. Soc. **1961**, 329. Y.-T. Lee and B. H. Mahan, J. Chem. Phys. **42**, 2893 (1965).

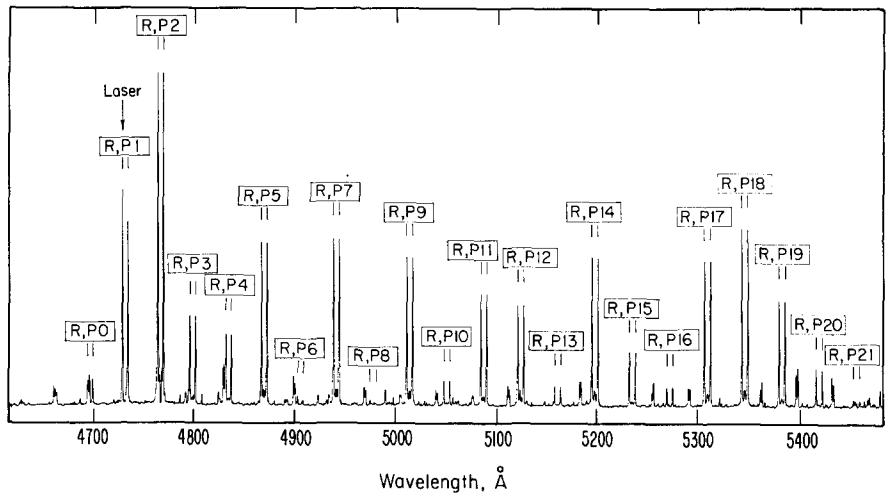

FIG. 2. Fluorescence spectrum of Na_2 excited by the argon-ion laser line $\lambda=4727$ Å. The prominent P and R doublet fluorescence progression, $(v'=9\ J'=38)\rightarrow(v'', J''=J'\pm1)$ has been marked $(P, R\ 0)$, $(P, R\ 1)$, $(P, R\ 2)$, $\cdots$, corresponding to the $v''=0$, $v''=1$, $v''=2$, $\cdots$, members of the fluorescence series. Note that this departs from the more traditional spectroscopic notation in order to designate the series in v''. The doublets correspond to $P(39)$ and $R(37)$.

ture of ground- and excited-state alkali dimers is the potential contributions such information can make to the interpretation of alkali scattering experiments. For example, a knowledge of the molecular potential curve over a wide range of internuclear distance is needed to calculate alkali spin exchange cross sections.[15] Moreover, because of the low binding energy of the alkali dimer and the high reactivity of the constituent alkali atoms, it is anticipated[16] that alkali dimers will become a popular reagent for crossed molecular beam experiments. Once again a knowledge of the forces between all collision partners is necessary for complete understanding of the results of such experiments.

We have emphasized so far the value of structural information about the alkali dimers, such as Na_2. We wish to stress as well the advantages inherent in the technique of laser-induced fluorescence. Absorption spectroscopy has long been the conventional means of obtaining molecular spectra.[17] However, this method is limited by its nature to the investigation of those ground state vibrational levels which are thermally populated. Moreover, for molecules like Na_2, which have large moments of inertia and small force constants, the absorption spectrum suffers from a superfluity of densely packed lines which cause so complex an appearance that analysis is often impeded and in some cases is altogether impossible. In the case of the Na_2 blue-green band systems, for example, the present values of the molecular constants are based on the work of Loomis and Wood,[18] who in 1928 photographed the absorption spectrum with a 40-ft spectrograph. Even with their attainable resolution of 0.03 Å, however, there remained many unresolved blends which could not be identified. Nevertheless, Loomis and Wood were able to determine with considerable accuracy the ground state values of the equilibrium rotational constant, B_e, and vibrational constant, ω_e, which characterize the lowest portion of the potential well. However, the dependence of their molecular constants on vibrational number was determined with much less certainty.

On the other hand, excitation of a single isolated upper level and analysis of the subsequent fluorescence represents a complementary technique which eliminates many of the difficulties associated with absorption spectroscopy. The fluorescence spectrum is simple in appearance and can be readily resolved. Moreover, we can obtain information about the high vibrational levels of the ground state.[19] If a sufficient number of fluorescence series can be found originating from different (v', J') levels of the upper state, a spectroscopic analysis of the excited state can be completed as well.

The use of laser lines as a light source to excite fluorescence is more than a mere extension of the use of metal arc lines. Because of the high intensity, directionality, and monochromaticity of the laser beam, whose wavelength can be chosen from a set of many possible laser transitions,[20] a particular vibrational–rotational level of the upper state can be appreciably populated. The resultant fluorescence is sufficiently intense that many different types of experiments, which otherwise would be extremely difficult, can be carried out with relative ease. One example is the use of laser-induced fluorescence to observe level crossings in the excited $B\ ^1\Pi_u$ state of the Na_2 molecule (see following

[15] See A. Dalgarno and M. R. H. Rudge, Proc. Roy. Soc. (London) **A286,** 519 (1965), and references contained therein.

[16] D. R. Herschbach (private communication).

[17] G. Herzberg, *Spectra of Diatomic Molecules* (D. Van Nostrand Co., Inc., Princeton, N.J., 1950).

[18] F. W. Loomis and R. W. Wood, Phys. Rev. **32,** 223 (1928). The vibrational analysis has been extended by the magnetic rotation work of F. W. Loomis and R. E. Nusbaum, *ibid.* **40,** 380 (1932).

[19] A striking example of the advantages of fluorescence spectroscopy in this regard is provided by the work of R. D. Verma [J. Chem. Phys. **32,** 738 (1960)], who was able to follow a resonance fluorescence progression in the I_2 molecule to the $v''=84$ vibrational level of the ground state, almost to the dissociation limit.

[20] For a recent compilation of the lines available from ion lasers see W. B. Bridges and A. N. Chester, IEEE J. Quantum Electron. **1,** 65 (1965).

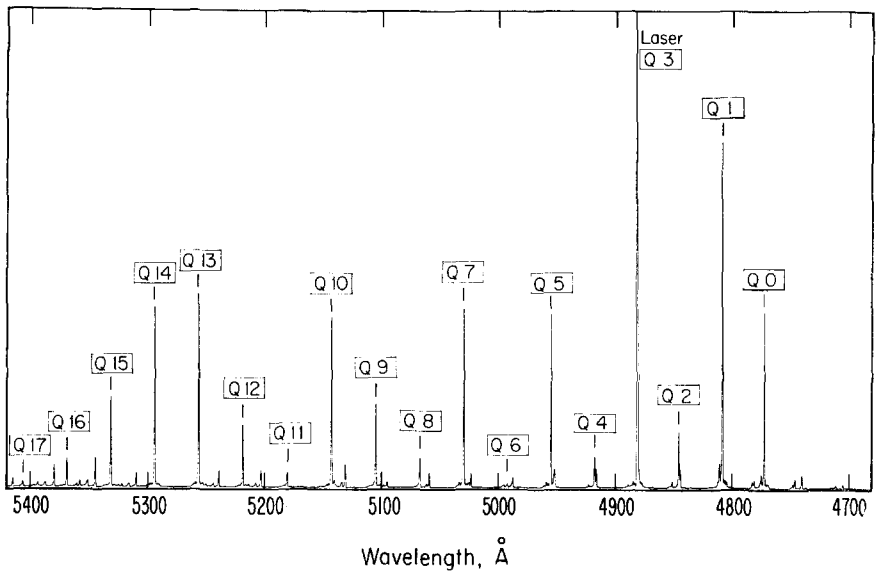

FIG. 3. Fluorescence spectrum of Na_2 excited by the argon-ion laser line $\lambda=4880$ Å. The prominent Q-line fluorescence progression ($v'=6$, $J'=43$)→(v'', $J''=43$) has been marked (Q 0), (Q 1), (Q 2), ···, corresponding to the $v''=0$, $v''=1$, $v''=2$, ···, members of the fluorescence series. The lines correspond to $Q(43)$ in standard notation.

paper). Another example is the interferometric determination[21] of the Na_2 fluorescent line positions which we report here.

II. EXPERIMENTAL

The experimental arrangement is shown in Fig. 1. The argon-ion laser, with a maximum output of about 800 mW at $\lambda=4880$ Å, can be tuned to the different cw-laser wavelengths using an internally reflecting prism P_1 as part of the laser resonant cavity. The laser beam passes through an external prism P_2 which ensures the spectral purity of the laser output and prevents plasma lines in the argon discharge from being transmitted through the optical stop into the fluorescence cell. The useful life of the fluorescence cell can be greatly prolonged by constructing it from Corning 1720 aluminosilicate glass.[22] We found we were able to operate the cell at a temperature of about 300°C for many tens of hours before discoloration interfered with our measurements. The cell's main body and reservoir, R, are separately heated by wrapping asbestos tape and nichrome wire about each. In order to prevent condensation of sodium vapor on the cell windows, the reservoir is maintained at a temperature about 10°C below the temperature of the cell. In addition, heater coils of the main cell are extended past each window. The atomic sodium partial pressure at the operating temperature of 280°C is about 6×10^{-3} torr and the Na_2 partial pressure is only about 4.4×10^{-5} torr.[3] Temperatures of the main body and of the reservoir of the fluorescence cell are monitored by thermocouples in contact with the glass cell.

The fluorescence is observed at right angles to the incident laser beam. Initially, a scanning monochromator (Ebert mount with a 1200-line/mm grating, 50-μ slits and a 0.5-Å resolution) was used to make a "map" of the fluorescence spectra excited by each laser line. The neon spectrum was superimposed to serve as a calibration.[23] These scans were then analyzed to determine the wavelength positions of the spectral lines to within 0.1 Å and to identify the members of each resonance fluorescence progression. This preliminary step to determine the wavelength positions of the fluorescence spectrum is a prerequisite to interferometric analysis.

Figures 2 and 3 show part of such a fluorescence map excited by the $\lambda=4727$-Å and $\lambda=4880$-Å laser lines, respectively. The relative intensities have not been corrected for the spectral response of the photomultiplier and the monochromator. Figure 2 shows that the 4727-Å laser line excites primarily a series of closely spaced P and R doublets ($\Delta J=\pm1$), and Fig. 3 shows that the 4880-Å laser line excites predominantly a series of Q lines ($\Delta J=0$). In both cases the fluorescence progressions can be followed to high-vibrational levels of the ground state.

To determine the wavelength positions of the fluorescence lines to a higher precision, a Fabry–Perot interferometer[24] with an etalon spacing of 0.3 cm and a finesse of approximately 10 over the entire spectral range covered is placed between the fluorescence cell and a Bass–Kessler type spectrograph of moderate dispersion (15 Å/mm), as shown in Fig. 1. By this means

[21] We wish to thank Dr. Richard L. Barger who proposed the technique of a Fabry–Perot interferometer crossed with a spectrograph to us one day over coffee. The only previous interferometric study of molecular fluorescence of which we are aware is the work of D. H. Rank and W. M. Baldwin [J. Chem. Phys. **19**, 1210 (1951)]. They investigated the I_2 fluorescence spectrum excited by the 5461-Å mercury green line.

[22] As described in Ref. 2(a).

[23] *American Institute of Physics Handbook*, D. E. Gray, Ed. (McGraw-Hill Book Co., New York, 1963), 2nd ed.

[24] M. Born and E. Wolf, *Principles of Optics* (Pergamon Press, Ltd., London, 1959).

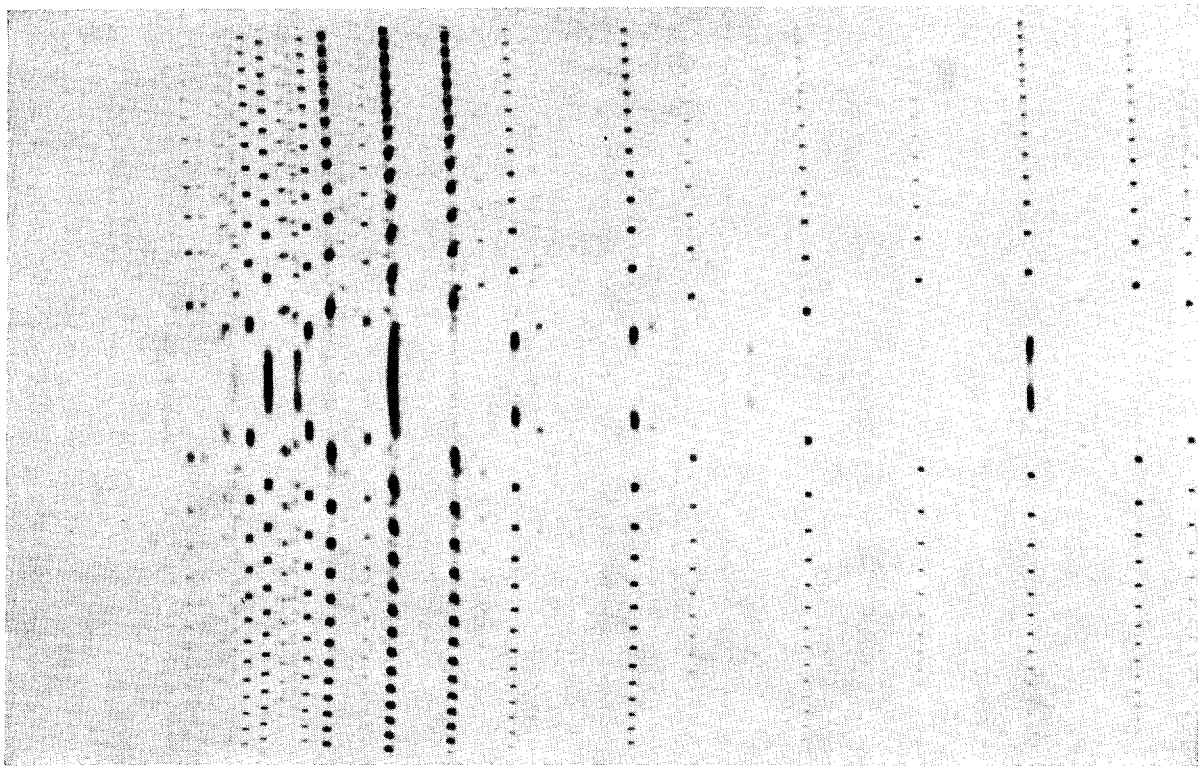

FIG. 4. Fabry–Perot fringe pattern dispersed with a plane-grating spectrograph, obtained from the Na_2 fluorescence spectrum shown in Fig. 3. Wavelength increases to the left.

TABLE I. Spectroscopic constants for the $X\,^1\Sigma_g^+$ ground state of the Na_2 molecule. The number of significant figures associated with each spectroscopic constant does not imply that the constant is known to that accuracy. The number of figures quoted allows calculation of the spectral line positions to the accuracy shown in Table IV.

Molecular constants[a]	Present work (cm^{-1})	Previous value[b] (cm^{-1})
ω_e	159.1268	159.23
$\omega_e x_e$	0.7262	0.726
$\omega_e y_e$	-9.154×10^{-4}	-2.7×10^{-3}
$\omega_e z_e$	-5.02×10^{-5}	...
B_e	0.154853[c]	0.15471
α_e	8.5637×10^{-4}	7.9×10^{-4}
γ_e	-7.646×10^{-6}	$-3.\times10^{-5}$
D_e	6.552×10^{-7}	5.84×10^{-7}
β_e	2.243×10^{-9}	$5.\times10^{-9}$
δ_e	2.0×10^{-10}	...

[a] For a definition see Eqs. (7), (9), and (10).

[b] As compiled by G. Herzberg in Ref. 17.

[c] This corresponds to an equilibrium internuclear distance of $r_e = 3.07745$ Å.

the entire fluorescence spectrum excited by a single-laser line is obtained on one photographic plate in most cases (Eastman–Kodak spectroscopic plate, emulsion type IV-F). When a Fabry–Perot interferometer is illuminated by monochromatic light, rings of bright and dark circles are produced which correspond to constructive and destructive interference of the emerging rays. If polychromatic light is incident on a Fabry–Perot interferometer, a complicated set of overlapping rings results from the superposition of the ring pattern belonging to each wavelength. If this light is sent through a spectrograph, the light beam is dispersed and a series of slit images of the ring pattern are formed on the focal plane of the instrument, the positions depending upon the incident wavelengths. Figure 4 is a reproduction of the fringe pattern which results when the Na_2 fluorescence spectrum excited by the 4880-Å laser line, shown in Fig. 3, is passed through this combination of a Fabry–Perot interferometer crossed with a spectrograph.

This photographed fringe pattern is measured with a high-precision microdensitometer comparator. From the observed fringe separations, the wavelengths of the lines can be determined by the method of exact fractions[24–26] which we will describe briefly. The fundamental condition for the appearance of a bright ring at an angle ϕ with respect to normal incidence is that

$$n\lambda = 2d\cos\phi, \tag{1}$$

[25] K. H. Meissner, J. Opt. Soc. Am. **31**, 405 (1941); **32**, 185 (1942).

[26] S. Tolansky, *An Introduction to Interferometry* (Longmans Green and Co., Ltd., London, 1955).

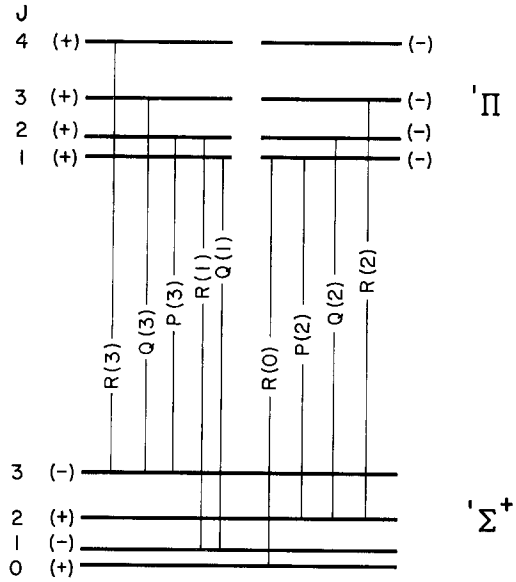

FIG. 5. Rotational energy-level diagram for a (v', v'') band of a $^1\Pi$–$^1\Sigma^+$ transition. For the sake of clarity only the first few lines are shown. The positive and negative levels have been marked (+) and (−), respectively.

where d is the spacer length of the Fabry–Perot etalon, λ is the wavelength of the incident light and n is an integer, called the order of the ring. It is possible to assign a nonintegral order number to any point between the rings. In particular, it is convenient to consider the order number N of the center of the ring pattern ($\phi=0$) for which

$$N\lambda=2d. \tag{2}$$

The real number N can be expressed as the sum of the integral order of the first bright ring n and a positive fraction ϵ,

$$N=n+\epsilon. \tag{3}$$

The integral order n can be determined if the wavelength position is known to within plus or minus half of the free spectral range of the Fabry–Perot interferometer. In the case of the Na_2 fluorescence spectrum this is obtained from the auxiliary photoelectric wavelength map. The fractional order ϵ can be determined from the measured fringe separations. If we call the ring diameter of the ith ring D_i, then

$$\epsilon=\frac{D_i^2}{(D_k^2-D_i^2)/(k-i)}-i. \tag{4}$$

In most cases, eight fringes were measured for each line, and a computer program was written to perform a best least-squares fit in determining ϵ. Once ϵ and n are known, Eqs. (1) and (2) can be combined to compute the value of the wavelength λ.

This method requires that the spacer distance d be known to better than one order of the Fabry–Perot interferometer. The precise Fabry–Perot plate separation is determined from a neon spectrum calibration plate which we made using the experimental setup pictured in Fig. 1. Actually, what is required for precise work is not the physical dimensions of the spacer but the optical path length between the plates. Because the dielectric coatings of the Fabry–Perot interferometer plates were multilayer coatings, the effective spacer distance was wavelength dependent. For our plates we found nearly one-half an order change from the maximum reflectivity at $\lambda_{max}=5150$ Å to the extremes of the spectral range covered (4700–5600 Å). A wavelength-dependent correction to the spacer length was accomplished by expressing the spacer distance as a quadratic function of the wavelength difference, $\lambda-\lambda_{max}$,

$$d(\lambda)=d_0+a(\lambda-\lambda_{max})+b(\lambda-\lambda_{max})^2, \tag{5}$$

and by determining the coefficients a and b of this expansion so that our observed fringe patterns for the neon spectrum reproduced the known neon wavelengths.[23] The wavelength-dependent spacing $d(\lambda)$ was then used in all subsequent determinations of the Na_2 fluorescent line wavelengths.

III. SPECTROSCOPIC ANALYSIS

An analysis of the Na_2 fluorescence series requires an understanding of the nature of the rotational levels in the two electronic states. Figure 5 illustrates the rotational structure of a $^1\Pi$–$^1\Sigma^+$ transition for which

TABLE II. Na_2 resonance fluorescence progressions excited by the lines of the argon-ion laser.

Laser wavelength in Å (air)[a]	Molecular transition excited v'	J'	v''	J''	Fluorescence intensity[b,c]	Highest v'' observed
4657.89	17	37	4	38	m	22
4726.86	9	38	1	37	s	21
	19	50	7	50	w	33
	13	10	4	9	w	25
4764.86	10	12	3	13	vs	23
	6	27	0	28	s	17
	10	91	1	91	w	24
4879.86	6	43	3	43	vs	19
	10	42	6	41	m	23
	7	99	2	99	m	23
	9	56	5	55	m	21
	15	97	7	98	mw	29
4965.07	7	43	6	44	m	18
	8	28	7	29	w	19
5017.16	5	37	6	38	m	15
5145.32	11	49	14	49	m	23
	2	84	6	85	m	10
	9	63	12	64	m	20
	9	96	11	97	w	16

[a] As calculated by Bridges and Chester in Ref. 20.

[b] The approximate power of the argon-ion laser lines was 20 mW at 4658 Å, 20 mW at 4727 Å, 30 mW at 4765 Å, 300 mW at 4880 Å, 25 mW at 4965 Å, 20 mW at 5017 Å, and 300 mW at 5145 Å.

[c] vs, very strong; s, strong; m, medium; mw, medium weak; w, weak.

there are three branches, P ($\Delta J=-1$), Q ($\Delta J=0$), and R ($\Delta J=+1$), corresponding to the rotational selection rules $\Delta J=0, \pm 1$. The rotational levels of each electronic state may be classified according to the behavior of the total molecular wavefunction with respect to inversion through the origin.[17] A rotational level is called *positive* or *negative* depending whether the parity of the total wavefunction is even or odd. For a $^1\Sigma^+$ electronic state, the diatomic molecule behaves as a simple rotor and the parity of the total wavefunction is determined solely by the parity of the rotational part. Accordingly, the rotational levels for the $^1\Sigma^+$ state have been marked in Fig. 5 (+) and (−) for even and odd J, respectively. For a $^1\Pi$ electronic state the diatomic molecule behaves as a symmetric top, and for each value of J there is a positive and negative rotational level (so-called Λ doublet) of equal energy, as pictured in Fig. 5. Actually, a splitting (Λ-type doubling) of these degenerate levels occurs because of the interaction between electronic and rotational motion. However, this splitting is so small in the case of Na_2 that its effect is neglected.[18]

The selection rules for dipole radiation only permit positive levels to combine with negative levels and vice versa. As a consequence, when the Na_2 molecule is irradiated with monochromatic light, it is excited to either the positive or the negative Λ-type doublet of a particular upper state (v', J') level, but not to both. It can then be seen from Fig. 5 that the resultant fluorescence spectrum consists of either P and R doublets, as in Fig. 2, or single Q lines, as in Fig. 3, but not P, Q, and R triplets from the same upper state (v', J') level. In what follows it will become apparent that the P and R doublet fluorescence series are much more useful in making a spectroscopic analysis of the $^1\Pi$–$^1\Sigma^+$ transition than are the Q-line fluorescence series.

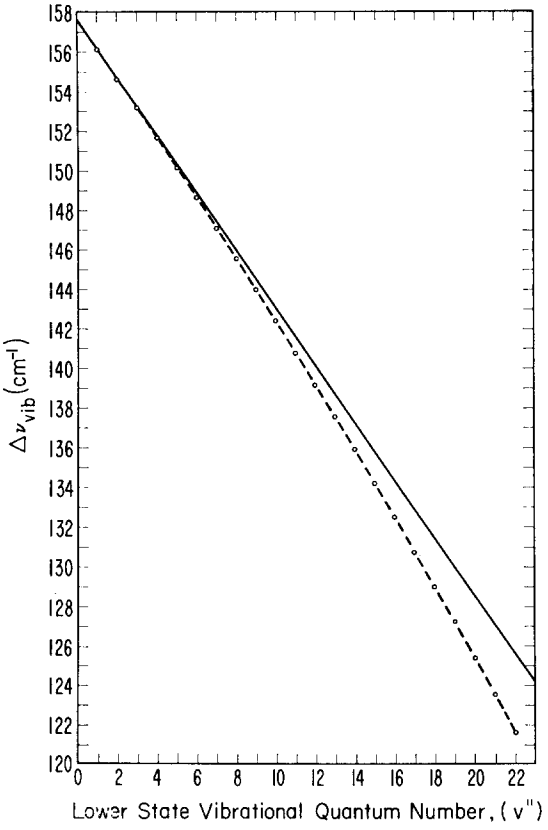

FIG. 6. A plot of $\Delta\nu_{vib}$ as a function of v''. The experimental values are shown by open circles and the best least-squares fit by a dashed line. A solid line has also been drawn with the limiting slope of the experimental points as they approach $v''=0$. The deviation of the experimental points from this straight line with increasing v'' is a measure of the magnitude of the molecular constants $\omega_e y_e$ and $\omega_e z_e$.

TABLE III. Spectroscopic constants for the $B\,^1\Pi_u$ excited state of the Na_2 molecule. The number of significant figures associated with each spectroscopic constant does not imply that the constant is known to that accuracy. The number of figures quoted allows calculation of the spectral line positions to the accuracy shown in Table IV.

Molecular constants[a]	Present work (cm^{-1})	Previous value[b] (cm^{-1})
T_e	20 319.596	20 320.2
ω_e	124.0656	123.79
$\omega_e x_e$	0.6863	0.6303
$\omega_e y_e$	-5.441×10^{-3}	-9.36×10^{-3}
$\omega_e z_e$	-1.15×10^{-4}	...
B_e	0.125829[c]	0.12588
α_e	8.6754×10^{-4}	9.4×10^{-4}
γ_e	-1.535×10^{-5}	
D_e	3.614×10^{-7}	
β_e	2.701×10^{-8}	
δ_e	-8.4×10^{-11}	

[a] For a definition see Eqs. (6), (7), (9), and (10).
[b] As compiled by G. Herzberg in Ref. 17.
[c] This corresponds to an equilibrium internuclear distance of $r_e=3.41398$ Å.

Because Na_2[23] is a homonuclear molecule, it possesses the additional symmetry of exchange in position of the identical nuclei.[17] Accordingly, the rotational levels may be further classified as *symmetric* or *antisymmetric* depending whether the total molecular wavefunction remains unchanged or changes sign under the exchange of the nuclei. For a $^1\Pi_u$–$^1\Sigma_g^+$ transition, however, this additional symmetry introduces no new prohibitions. The positive and negative rotational levels of the $^1\Sigma_g^+$ electronic state are symmetric and antisymmetric, respectively, whereas in the $^1\Pi_u$ electronic state the designations are reversed. The selection rule that symmetric levels can only combine with symmetric levels and antisymmetric levels with antisymmetric levels is thus equivalent to the selection rule that positive levels can only combine with negative levels and vice versa.

The line positions $\nu(v''J''; v'J')$ of a fluorescence series may be represented by the energy difference between the (v', J') and (v'', J'') vibrational-rotational

TABLE IV. Frequencies (wavenumbers) for some interferometrically measured lines of P and R fluorescence series of Na_2.

v''	ν_{obs} (cm^{-1})	ν_{calc} (cm^{-1})	Δ (cm^{-1})
	The (9, 38→v'', 37) R series		
0	21 306.214	21 306.227	−0.013
1	149.780	149.787	−0.007
2	20 994.811	994.831	−0.020
3	841.322	841.367	−0.045
4	689.338	689.404	−0.066
5	538.873	538.953	−0.080
6	389.931	390.026	−0.095
7	242.521	242.634	−0.113
8	096.670	096.792	−0.122
9	19 952.396	19 952.515	−0.119
10	809.706	809.820	−0.114
11	668.614	668.723	−0.109
12	19 529.128	19 529.243	−0.115
13	391.278	391.402	−0.124
14	255.095	255.219	−0.124
15	120.589	120.717	−0.128
16	18 987.796	18 987.919	−0.123
17	856.740	856.851	−0.111
18	727.440	727.539	−0.099
19	599.940	600.009	−0.069
20	474.265	474.289	−0.024
21	350.426	350.411	+0.015
	The (9, 38→v'', 39) P series		
0	21 282.726	21 282.745	−0.019
1	126.416	126.441	−0.025
2	20 971.588	20 971.623	−0.035
3	818.250	818.299	−0.049
4	666.402	666.480	−0.078
5	516.079	516.175	−0.096
6	367.286	367.395	−0.109
7	220.029	220.154	−0.125
8	074.326	074.465	−0.139
9	19 930.203	19 930.344	−0.141
10	787.671	787.807	−0.136
11	646.741	646.871	−0.130
12	507.409	507.555	−0.146
13	369.725	369.879	−0.154
14	233.757	233.865	−0.108
15	099.384	099.533	−0.149
16	18 966.762	966.910	−0.148
17	835.864	836.018	−0.154
18	706.742	706.884	−0.142
19	579.442	579.535	−0.093
20	453.945	453.999	−0.054
21	330.297	330.306	−0.009
	The (10, 12→v'', 11) R series		
0	21 456.983	21 456.977	+0.006
1	299.416	299.421	−0.005
2	143.294	143.329	−0.035
3	20 988.653	20 988.709	−0.056
4	835.495	835.570	−0.075
5	683.835	683.923	−0.088
6	533.689	533.778	−0.089
7	385.063	385.149	−0.086
8	237.972	238.049	−0.077
9	092.431	092.494	−0.063
10	19 948.454	948.501	−0.047
11	806.066	806.086	−0.020
12	665.270	665.268	+0.002
13	526.088	526.067	+0.021
14	388.532	388.505	+0.027
15	252.628	252.604	+0.024
16	118.414	118.387	+0.027
17	18 985.908	18 985.879	+0.029
18	855.144	855.106	+0.038
19	726.122	726.096	+0.026
20	598.878	598.876	+0.002
21	473.460	473.476	−0.016
22	349.879	349.927	−0.048
23	228.218	228.262	−0.044
	The (10, 12→v'', 13) P series		
0	21 449.278	21 449.267	+0.011
1	291.747	291.754	−0.007
2	135.672	135.706	−0.034
3	20 981.071	20 981.132	−0.061
4	827.962	828.039	−0.077
5	676.347	676.438	−0.091
6	526.251	526.340	−0.091
7	377.678	377.760	−0.082
8	230.627	230.709	−0.082
9	085.141	085.204	−0.063
10	19 941.215	19 941.261	−0.046
11	798.875	798.897	−0.022
12	658.129	658.131	−0.002
13	519.006	518.983	+0.023
14	381.510	381.475	+0.035
15	245.660	245.628	+0.032
16	111.500	111.467	+0.033
17	18 979.048	18 979.015	+0.033
18	848.336	848.298	+0.038
19	719.372	719.345	+0.027
20	592.185	592.184	+0.001
21	466.825	466.843	−0.018
22	343.319	343.354	−0.035
23	221.708	221.749	−0.041
	The (6, 27→v'', 26) R series		
0	20 997.861	20 997.811	+0.050
1	840.799	840.753	+0.046
2	685.220	685.168	+0.032
3	531.115	531.064	+0.051
4	378.486	378.450	+0.036
5	227.360	227.336	+0.024
6	077.769	077.734	+0.035
7	19 929.694	19 929.657	+0.037
8	783.153	783.118	+0.035
9	638.168	638.132	+0.036
10	494.760	494.717	+0.043
11	352.946	352.889	+0.057
12	212.730	212.667	+0.063
13	074.125	074.072	+0.053
14	18 937.184	18 937.123	+0.061
15	801.918	801.845	+0.073
16	668.344	668.259	+0.085
17	536.478	536.392	+0.086
	The (6, 27→v'', 28) P series		
0	20 980.970	20 980.934	+0.036
1	824.024	823.972	+0.052
2	668.540	668.485	+0.055
3	514.529	514.481	+0.048
4	20 362.016	20 361.969	+0.047
5	211.000	210.958	+0.042
6	061.514	061.461	+0.053
7	19 913.531	913.491	+0.040
8	767.091	767.060	+0.031
9	622.226	622.185	+0.041
10	478.919	478.882	+0.037
11	337.203	337.167	+0.036
12	197.099	197.061	+0.038
13	058.620	058.583	+0.037
14	18 921.800	18 921.754	+0.046
15	786.653	786.596	+0.057
16	653.190	653.133	+0.057
17	521.467	521.390	+0.077

TABLE IV (*Continued*)

v''	ν_{obs} (cm^{-1})	ν_{calc}(cm^{-1})	Δ (cm^{-1})	v''	ν_{obs} (cm^{-1})	ν_{calc}(cm^{-})	Δ (cm^{-1})
	The (10, 42→v'', 41) R series				The (10, 42→v'', 43) P series		
0	21 401.078	21 401.118	−0.040	0	21 375.208	21 375.270	−0.062
1	244.945	244.956	−0.011	1	219.240	219.257	−0.017
2	090.295	090.283	+0.012	2	064.755	064.737	+0.018
3	20 937.145	20 937.108	+0.037	3	20 911.761	20 911.717	+0.044
4	785.502	785.439	+0.063	4	760.274	760.207	+0.067
5	635.367	635.287	+0.080	5	610.307	610.216	+0.091
6	486.753	486.664	+0.089	6	461.855	461.757	+0.098
7	339.670	339.581	+0.089	7	314.945	314.841	+0.104
8	194.138	194.054	+0.084	8	169.580	169.484	+0.096
9	050.173	050.097	+0.076	9	025.783	025.699	+0.084
10	19 907.789	19 907.727	+0.062	10	19 883.570	19 883.504	+0.066
11	767.008	766.960	+0.048	11	742.958	742.916	+0.042
12	627.829	627.816	+0.013	12	19 603.959	19 603.953	+0.006
13	490.304	490.315	−0.011	13	466.610	466.636	−0.026
14	354.456	354.478	−0.022	14	330.941	330.986	−0.045
15	220.296	220.328	−0.032	15	196.948	197.025	−0.077
16	087.841	087.887	−0.046	16	064.705	064.776	−0.071
17	18 957.140	18 957.180	−0.040	17	18 934.190	18 934.266	−0.076
18	828.215	828.235	−0.020	18	805.455	805.518	−0.063
19	701.087	701.077	+0.010	19	678.518	678.561	−0.043
20	575.792	575.735	+0.057	20	553.428	553.423	+0.005
21	452.368	452.239	+0.129	21	430.209	430.134	+0.075
22	330.833	330.619	+0.214	22	308.905	308.724	+0.181

levels of the excited and ground states[17]:

$$\nu(v''J''; v'J') = T_e + [G(v') - G(v'')] + [F_{v'}(J') - F_{v''}(J'')], \quad (6)$$

where

$$G(v) = \omega_e(v+\tfrac{1}{2}) - \omega_e x_e(v+\tfrac{1}{2})^2 + \omega_e y_e(v+\tfrac{1}{2})^3 + \omega_e z_e(v+\tfrac{1}{2})^4 + \cdots \quad (7)$$

and

$$F_v(J) = B_v[J(J+1) - \Lambda^2] - D_v[J(J+1) - \Lambda^2]^2 + \cdots. \quad (8)$$

The first term, T_e, in Eq. (6) is the electronic energy separation between the ground and excited states (the separation between the minima of the two potential curves), the second term expresses the vibrational energy difference, and the last term represents the energy difference between the rotational levels in the upper and lower vibrational states. In Eq. (7) the vibrational energy, $G(v)$, is given by a series expansion in powers of $(v+\frac{1}{2})$, where v is the vibrational quantum number. In Eq. (8) the rotational energy in the vibrational level v, $F_v(J)$, is given by a series expansion in powers of $[J(J+1)-\Lambda^2]$, where J is the rotational quantum number and Λ is the absolute value of the projection of the electronic angular momentum upon the internuclear axis. For a Σ state $\Lambda=0$, whereas for a Π state $\Lambda=1$. The rotational constants B_v and D_v depend upon the vibrational level v and can be represented by another power series in $(v+\frac{1}{2})$:

$$B_v = B_e - \alpha_e(v+\tfrac{1}{2}) + \gamma_e(v+\tfrac{1}{2})^2 + \cdots \quad (9)$$

and

$$D_v = D_e + \beta_e(v+\tfrac{1}{2}) + \delta_e(v+\tfrac{1}{2})^2 + \cdots. \quad (10)$$

The task of a spectroscopic analysis is then to determine the unknown molecular constants ω_e, $\omega_e x_e$, $\omega_e y_e$, $\omega_e z_e$, B_e, α_e, γ_e, D_e, β_e, δ_e, etc., for both the ground and excited states from the measured positions of the molecular lines.

The first step is to identify the correct v'', J'' and v', J' quantum numbers which are to be assigned to a line. In the case of the blue-green bands of Na_2 this is greatly facilitated by the previous absorption work[18] which furnishes approximate values of ω_e, $\omega_e x_e$, B_e, and α_e for the ground and excited states.[27] From Eqs. (6)–(10) the spacing between two lines (v'', J'') and $(v''+1, J'')$ of the same fluorescence progression is given by

$$\Delta\nu_{vib}(v) = a_0 - a_1 v + a_2 v^2 + a_3 v^3 + \cdots, \quad (11)$$

where

$$a_0 = \omega_e - 2\omega_e x_e + 3.25\omega_e y_e + 5\omega_e z_e + (-\alpha_e + 2\gamma_e)J(J+1) - (\beta_e + 2\delta_e)[J(J+1)]^2,$$

$$a_1 = 2\omega_e x_e - 6\omega_e y_e - 13\omega_e z_e - \gamma_e J(J+1) + 2\delta_e[J(J+1)]^2,$$

$$a_2 = 3\omega_e y_e + 12\omega_e z_e,$$

$$a_3 = 4\omega_e z_e. \quad (12)$$

Equations (6), (11), and (12) then permit us to assign the values of v' and v'' to a line based on the previously determined spectroscopic constants.[17,18] Figure 6 shows an example of a plot of $\Delta\nu_{vib}$ as a function of v''. It is clear from this figure that an error by one vibrational unit in v'' would cause a change in the intercept of about 1.5 cm^{-1}, which is outside the experimental uncertainty of the spectroscopic constants. The correct

[27] The rotational and vibrational assignments can in principle be made without previous knowledge of the spectrum [see Ref. 2(a)].

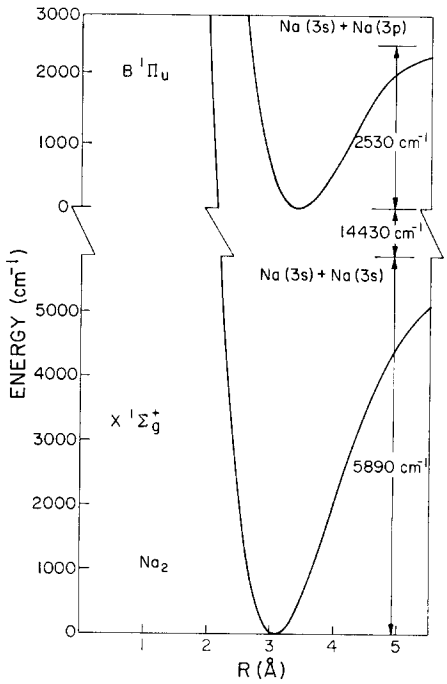

FIG. 7. Potential energy curves for the X and B states of Na_2 constructed by the RKR method.

v'' value can also be determined approximately from the number of antistokes lines (i.e., fluorescent lines with wavelengths shorter than the exciting laser line). This determination can also be confirmed in a later stage of the analysis by comparing the measured line intensities with the calculated Franck–Condon factors, which gives a very sensitive check on the correctness of the vibrational numbering.

The question of the correct rotational numbering is, in general, more difficult to settle, especially for a Q-line series. Figure 5 shows that the energy spacings between Q lines that differ by one unit in J are quite small. Consequently, unless the spectroscopic constants are already known to high accuracy, which was not the case in Na_2, the Q series do not allow an independent determination of the rotational and vibrational quantum number from Eqs. (11) and (12). For this reason the initial analysis is restricted to P and R series. From Eqs. (6)–(10) the spacing between the two doublet members $(v'', J'+1)$ and $(v'', J'-1)$ of a P and R fluorescence series is given by

$$\Delta\nu_{\rm rot}(v) = b_0 - b_1 v + b_2 v^2, \tag{13}$$

where

$$b_0 = (4B_e - 2\alpha_e + \gamma_e - 6D_e - 3\beta_e - 1.5\delta_e)(J'+\tfrac{1}{2}) - (8D_e + 4\beta_e + 2\delta_e)(J'+\tfrac{1}{2})^3,$$

$$b_1 = (4\alpha_e - 4\gamma_e + 6\beta_e + 6\delta_e)(J'+\tfrac{1}{2}) + 8\beta_e(J'+\tfrac{1}{2})^3,$$

$$b_2 = (4\gamma_e - 6\delta_e)(J'+\tfrac{1}{2}) - 8\delta_e(J'+\tfrac{1}{2})^3. \tag{14}$$

By making a least-squares fit of $\Delta\nu_{\rm rot}$ against v the coefficients b_0, b_1 and b_2 may be obtained for a particular P and R fluorescence series. The rotational numbering could then be determined from these coefficients, shown in Eq. (14), and from the vibrational coefficients a_0 and a_1 given in Eq. (12). Since the dependence of a_0 on J is quadratic (neglecting small fourth-order corrections) whereas the dependence of b_0 on J is linear (neglecting small third-order corrections), the value of J may be established even if no previously determined constants are known, provided the precision of the measurements is sufficiently high.

As more and more fluorescence series are identified and assigned v', J' and v'', J'' quantum numbers, Eqs. (11)–(14) may be used to improve the spectroscopic constants for the ground state by making a least-squares fit to all the lines in the different series. Table I gives the best values of the ground-state molecular constants based on five different P and R fluorescence series. A comparison with the previously determined ground-state spectroscopic constants, also given in Table I, shows that the values of ω_e, B_e, and $\omega_e x_e$ are little changed. However, a major improvement has been made in expressing the vibrational dependence of the $G(v)$ and B_v values in the present analysis. Note that the ground-state molecular constants we have found using Eqs. (11)–(14) are *independent* of the values of the upper-state constants.

These revised spectroscopic constants are used in turn to identify and assign additional fluorescence series for which the use of previous spectroscopic con-

TABLE V. Potential energy of the $X\,^1\Sigma_g^+$ state of Na_2 ($J=0$ rotational level).

$I=v+\frac{1}{2}$	U (cm^{-1})	r_- (Å)	r_+ (Å)
0.0	0.0	3.0774	
0.5	79.382	2.9473	3.2193
1.5	237.053	2.8586	3.3316
2.5	393.262	2.8006	3.4137
3.5	548.001	2.7552	3.4835
4.5	701.262	2.7172	3.5463
5.5	853.032	2.6842	3.6045
6.5	1003.302	2.6548	3.6594
7.5	1152.058	2.6282	3.7119
8.5	1299.287	2.6039	3.7625
9.5	1444.973	2.5815	3.8117
10.5	1589.100	2.5607	3.8597
11.5	1731.651	2.5412	3.9068
12.5	1872.606	2.5229	3.9532
13.5	2011.946	2.5057	3.9990
14.5	2149.650	2.4893	4.0445
15.5	2285.694	2.4738	4.0896
16.5	2420.057	2.4590	4.1344
17.5	2552.712	2.4449	4.1792
18.5	2683.635	2.4313	4.2239
19.5	2812.797	2.4184	4.2687
20.5	2940.171	2.4059	4.3136
21.5	3065.726	2.3938	4.3586
22.5	3189.432	2.3822	4.4040
23.5	3311.258	2.3710	4.4496

stants led to ambiguity. In particular, once the rotational constants have been established to high precision, Eqs. (10) and (11) can be used to determine the correct rotational numbering of the Q series. Table II presents the Na_2 fluorescence series that were excited using the different lines of the argon-ion laser. This represents a complete compilation in that we were able to identify and assign all fluorescence series which were of sufficient intensity to allow us to measure accurately a number of fluorescent line positions. We also list in Table II the relative strengths of the different fluorescent series, the highest vibrational level to which we could follow the fluorescence progression and the quantum numbers of the lower and upper states involved in the excitation caused by the argon-ion laser line.

Once the ground-state molecular constants are known, the excited-state molecular constants may be determined from the values of the ground-state constants in the following manner: Each fluorescence series originates from a particular (v', J') level of the excited state. With the measured frequencies $\nu(v'J'; v''J'')$ of the fluorescent lines Eq. (6) may be used to find the value of $E(v', J')=T_e+G(v')+F_{v'}(J')$ for the (v', J') level of the upper state. A least-squares fit to powers of $(v'+\frac{1}{2})$ and $[J'(J'+1)-1]$ may then be made to find the desired upper-state constants. A useful simplification of this procedure results when fluorescence series originate from more than one rotational level of the *same* upper-state vibrational level, in which case the difference between $E(v', J_1')-E(v', J_2')$ will depend only on the values of $B_{v'}$ and $D_{v'}$. For the Na_2 $B\,{}^1\Pi_u$ state, examination of Table II shows that the $v'=6$, 7, 9, and 10 vibrational levels are responsible for more than one fluorescence series. This then permits the determination of B_6, B_7, B_9, and B_{10} as well as D_6, D_7, D_9, D_{10}. The values of these rotational constants were combined with the values of B_0, B_1, D_0, and D_1 determined previously by absorption spectroscopy.[18,28]

TABLE VI. Potential energy of the $B\,{}^1\Pi_u$ state of Na_2 ($J=0$ rotational state).

$I=v+\frac{1}{2}$	U (cm^{-1})	r_- (Å)	r_+ (Å)
0.0	0.0	3.4140	
0.5	61.861	3.2673	3.5755
1.5	184.535	3.1683	3.7048
2.5	305.785	3.1041	3.8000
3.5	425.571	3.0542	3.8818
4.5	543.854	3.0126	3.9560
5.5	660.588	2.9767	4.0254
6.5	775.729	2.9450	4.0915
7.5	889.226	2.9165	4.1554
8.5	1001.027	2.8906	4.2176
9.5	1111.078	2.8667	4.2787
10.5	1219.321	2.8447	4.3391

[28] The values of D_0 and D_1 reported by Loomis and Wood in Ref. 18 are a factor of 10 too large due to a typographical error.

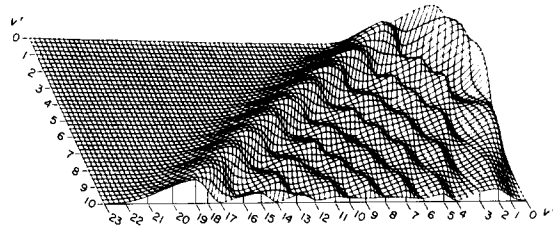

FIG. 8. Condon diagram for the Na_2 $B\,{}^1\Pi_u$–$X\,{}^1\Sigma_g^+$ band system. The height of each v', v'' intersection corresponds to the magnitude of the $q_{v'v''}$ Franck–Condon factor. Extra lines have been drawn in by interpolation between each integral value of v in order to enhance the features of the surface map.

The rotational constants B_e, α_e, γ_e, D_e, β_e, and δ_e of the upper state were then found by making a least-squares fit of the $B_{v'}$ and $D_{v'}$ values as a function of $(v'+\frac{1}{2})$. From these rotational constants we could evaluate $F_{v'}(J')$ and hence, from $E(v', J')$ the value of $T_e+G(v')$ for each fluorescence series. A least-squares fit of the values of $T_e+G(v')$ against $(v'+\frac{1}{2})$ provided the remaining unknown upper state constants.

The spectroscopic constants for the upper state are collected in Table III where they are compared with the previously reported values. Once again a significant improvement has been made in the dependence of the $G(v)$ and B_v values upon vibrational numbering. In order to check the molecular constants given in Tables I and III, they have been used to calculate the fluorescent line positions of several P and R fluorescence series whose lines have been interferometrically measured. The results of this test are presented in Table IV. From a comparison of the calculated and observed line positions in Table IV we conclude that the revised spectroscopic constants given in Tables I and III are able to reproduce the known line positions to better than 0.1 cm^{-1} in most cases. Similar tests have been carried out for some interferometrically measured Q-line fluorescence series with, on the whole, very satisfactory results. However, we have found that the Q series are not fitted quite as well as the P and R series, particularly for high rotational quantum numbers. This suggests a small Λ-type splitting in the $^1\Pi_u$ excited state, but we did not feel sufficiently confident of our upper state constants for high J to pursue this matter further.[29]

It might be conjectured that the new spectroscopic constants reported here are only marginally superior to the previous values given in Tables I and III. This is certainly not the case. Although the previous spectroscopic constants fit best for small values of v'' and J'', they deviate from the observed spectral line positions

[29] In Ref. 18 Loomis and Wood find a combination defect of 1×10^{-5} in the B values arising from the Q branches and the P and R branches. If this deviation is real, an error of 0.1 cm^{-1} in the line position results if the spectroscopic constants found from P and R series are used to calculate Q-line positions for $J=100$.

TABLE VII. Franck–Condon factors for the $B\,^1\Pi_u$–$X\,^1\Sigma_g^+$ band system of Na_2.

v''	$v'=0$	$v'=1$	$v'=2$	$v'=3$	$v'=4$	$v'=5$	$v'=6$	$v'=7$	$v'=8$	$v'=9$	$v'=10$
0	6.55 −2	1.61 −1	2.13 −1	2.00 −1	1.51 −1	9.77 −2	5.61 −2	2.94 −2	1.44 −2	6.64 −3	2.94 −3
1	1.93 −1	1.92 −1	5.53 −2	2.47 −4	4.52 −2	1.03 −1	1.23 −1	1.07 −1	7.68 −2	4.83 −2	2.75 −2
2	2.69 −1	4.05 −2	3.19 −2	1.15 −1	7.40 −2	8.32 −3	9.19 −3	5.28 −2	8.78 −2	9.42 −2	7.92 −2
3	2.35 −1	1.67 −2	1.30 −1	2.68 −2	1.69 −2	8.17 −2	6.84 −2	1.56 −2	1.46 −3	2.92 −2	6.30 −2
4	1.43 −1	1.36 −1	4.39 −2	3.84 −2	9.15 −2	1.41 −2	1.53 −2	6.60 −2	5.99 −2	1.81 −2	a
5	6.44 −2	1.96 −1	9.62 −3	1.08 −1	2.86 −3	5.45 −2	6.53 −2	5.72 −3	1.66 −2	5.69 −2	5.22 −2
6	2.22 −2	1.49 −1	1.16 −1	2.24 −2	6.54 −2	5.29 −2	3.20 −3	6.06 −2	4.46 −2	1.45 −3	1.84 −2
7	5.95 −3	7.41 −2	1.77 −1	2.28 −2	8.28 −2	6.65 −3	7.60 −2	1.46 −2	1.68 −2	5.78 −2	2.88 −2
8	1.26 −3	2.63 −2	1.33 −1	1.31 −1	2.55 −3	8.92 −2	9.94 −3	4.16 −2	5.20 −2	6.53 −4	2.96 −2
9	2.09 −4	6.96 −3	6.34 −2	1.65 −1	5.53 −2	4.26 −2	4.37 −2	4.98 −2	4.28 −3	5.69 −2	2.42 −2
10		1.40 −3	2.11 −2	1.08 −1	1.51 −1	5.87 −3	8.21 −2	4.38 −3	6.78 −2	6.62 −3	2.74 −2
11		2.15 −4	5.10 −3	4.57 −2	1.45 −1	1.02 −1	6.11 −3	8.10 −2	6.55 −3	4.60 −2	3.57 −2
12			9.18 −4	1.34 −2	7.90 −2	1.59 −1	4.41 −2	4.02 −2	4.59 −2	3.72 −2	1.23 −2
13			1.24 −4	2.81 −3	2.80 −2	1.15 −1	1.43 −1	6.43 −3	7.37 −2	1.01 −2	6.07 −2
14				4.34 −4	6.92 −3	4.98 −2	1.43 −1	1.03 −1	2.51 −3	8.10 −2	6.92 −4
15					1.22 −3	1.44 −2	7.75 −2	1.56 −1	5.50 −2	2.63 −2	5.93 −2
16					1.56 −4	2.92 −3	2.65 −2	1.07 −1	1.48 −1	1.64 −2	5.83 −2
17						4.17 −4	6.14 −3	4.38 −2	1.34 −1	1.21 −1	1.98 −4
18							9.87 −4	1.17 −2	6.60 −2	1.52 −1	8.09 −2
19							1.11 −4	2.11 −3	2.03 −2	9.17 −2	1.56 −1
20								2.63 −4	4.14 −3	3.28 −2	1.18 −1
21									5.73 −4	7.57 −3	4.95 −2
22										1.16 −3	1.30 −2
23										1.26 −4	2.22 −3

[a] Less than 1×10^{-4}.

with increasing values of v'' or J''. In particular, if the previous spectroscopic constants are used to compute the fluorescent line positions given in Table IV, errors on the average of about 9 cm^{-1} result. This is nearly 100 times the spectroscopic error of the revised constants and far outside our experimental uncertainty.[30]

IV. POTENTIAL CURVES AND FRANCK–CONDON FACTORS

The potential curves for the $X\,^1\Sigma_g^+$ and $B\,^1\Pi_u$ states of Na_2 have been constructed from the spectroscopic constants given in Tables I and III using the Rydberg–Klein–Rees (RKR)[31–33] method. In this semiclassical procedure the turning points r_+ and r_- of the classical motion of the molecule are determined for each vibrational energy level U from the expression

$$r_\pm(U)=(f/g+f^2)^{1/2}\pm f, \tag{15}$$

where f and g are given by

$$f(U)=\frac{1}{2\pi(2\mu)^{1/2}}\int_0^{I'}[U-E(I,\kappa)]^{-1/2}dI \tag{16}$$

and

$$g(U)=\frac{1}{2\pi(2\mu)^{1/2}}\int_0^{I'}\frac{\partial E}{\partial\kappa}[U-E(I,\kappa)]^{-1/2}dI. \tag{17}$$

Here $E(I,\kappa)$ is the energy function of the molecule in terms of the radial and angular momentum action variables $I=h(v+\frac{1}{2})$ and $\kappa=J(J+1)h^2/8\pi^2\mu$, respectively, and μ is the reduced mass of the molecule. Equations (16) and (17) are to be evaluated for $\kappa=0$ to construct the effective potential function for the nonrotating ($J=0$) molecule. The integrands in Eqs. (16) and (17) are singular at the upper limit of integration where $E(I',\kappa)=U$. In the past this has been a source of considerable difficulty in applying the RKR method. However, this mathematical problem can be overcome by using numerical methods and computer codes which are fully described elsewhere.[34]

In Tables V and VI we present the turning points for the X and B states. The calculations have been carried out as far as known spectroscopic data would permit, i.e., to the 23rd vibrational level of the ground state and to the 10th vibrational level of the upper state. It is possible to extend the turning point calculations to still higher vibrational levels but this would require an extrapolation of the available rotational data. The potential curves for the X and B states are obtained from the data in Tables V and VI by connect-

[30] It should be noted that in principle, the resolution of the Fabry–Perot interferometer crossed with a spectrograph is capable of measuring the position of a spectral line to some fraction of its Doppler width. However, in these studies we have not attempted to exploit the full resolution obtainable with this instrumental combination.

[31] R. Rydberg, Ann. Physik **73,** 376 (1931).

[32] O. Klein, Z. Physik **76,** 226 (1932).

[33] A. L. G. Rees, Proc. Phys. Soc. (London) **A59,** 998 (1947).

[34] R. N. Zare, University of California Radiation Laboratory Report, UCRL-10925, 1963; J. Chem. Phys. **40,** 1934 (1964); J. I. Steinfeld, R. N. Zare, L. Jones, M. Lesk, and W. Klemperer, *ibid.* **42,** 25 (1965). R. N. Zare, E. O. Larsson, and R. A. Berg, J. Mol. Spectry. **15,** 117 (1965).

ing the turning points with a smooth curve. To estimate the form of the potential curve outside of the turning point data, repulsive and attractive segments are smoothly joined to the central portion. In these regions the potential is assumed to have the form

$$V_{\text{rep}}=a/r^{12}+b \tag{18}$$

and

$$V_{\text{att}}=c/r^{d}, \tag{19}$$

where the zero of the potential energy is taken to be the dissociation energy of the molecule. The constants a, b, c, and d in Eqs. (18) and (19) are determined from the last two pairs of RKR turning points. Figure 7 shows the form of the potential curves for the Na_2 $X\,{}^1\Sigma_g^+$ and Na_2 $B\,{}^1\Pi_u$ electronic states as a function of the internuclear distance r.

Once an accurate potential curve $V(r)$ has been constructed it may be used to calculate various properties that depend on the nuclear motion of the molecule, in particular the relative fluorescence line intensities.[34] To a first approximation, the observed fluorescence rate from the upper-state level (v', J') to the ground-state levels (v'', J'') depends upon the population of excited molecules in the (v', J') level and the spontaneous emission coefficient $A(v'J'\rightarrow v''J'')$ for the transition. Thus the ratio of intensities, measured in energy per second, for two members of the same fluorescence series is given by

$$\frac{I_{v_1J}}{I_{v_2J}}=\frac{A(v'J'\rightarrow v_1J)}{A(v'J'\rightarrow v_2J)}. \tag{20}$$

Using the Born–Oppenheimer approximation[17] and assuming that the electronic transition moment is constant over the molecular band system, the fluorescence intensity ratio in Eq. (20) may be rewritten

$$\frac{I_{v_1J}}{I_{v_2J}}=\frac{\nu^4(v'J'\rightarrow v_1J)\,q(v'J';\,v_1J)}{\nu^4(v'J'\rightarrow v_2J)\,q(v'J';\,v_2J)}. \tag{21}$$

Here ν is the frequency of the transition and q is the Franck–Condon factor for the transition defined as the square of the vibrational overlap integral

$$q(v'J';\,v''J'')=\left(\int \psi_{v'J'}\psi_{v''J''}dr\right)^2, \tag{22}$$

where $\psi_{v'J'}$ and $\psi_{v''J''}$ are the upper- and lower-state vibrational wavefunctions which satisfy the radial Schrödinger equation

$$(d^2\psi_{vJ}/dr^2)+\{E_{vJ}-V(r)+[J(J+1)h^2/8\pi^2\mu r^2]\}\psi_{vJ}=0 \tag{23}$$

for the potential $V(r)$ with vibrational eigenvalues E_{vJ}. Using the potential curves shown in Fig. 6 we have evaluated Franck–Condon factors for all (v', v'') bands for which we trust the form of our potential curves.[35]

The resultant Franck–Condon factor array is presented in Table VII. The negative number in each entry is the power of 10 by which the entry has to be multiplied (e.g., 1.23 −4 stands for 1.23×10^{-4}). Values smaller than 1.00×10^{-4} have been omitted. The Franck–Condon factors given in Table VII have been calculated from rotationless $(J=0)$ potentials and strictly apply to the hypothetical $Q(0)$ line of the band. However, this approximation introduces an error of less than 5% in the value of the Franck–Condon factors computed for $J=40$, for example.

From Eq. (21) it is seen that the fluorescence intensity ratio depends upon the frequency ν, and the Franck–Condon factor, q. While the frequency factor is a smoothly varying function over the fluorescence progression, Table VII shows that the Franck–Condon factor is an extremely sensitive function of the relative phase of the two oscillatory vibrational wavefunctions and varies irregularly, often by more than two orders of magnitude, from line to line of the fluorescence progression. We conclude then that it is primarily the magnitude of the Franck–Condon factors that controls the intensity pattern of a resonance fluorescence series.

The large array of numbers presented in Table VII is difficult to grasp all at one time. To show the broad features of the Franck–Condon array we have prepared an isometric plot (Fig. 8) of the Franck–Condon factors in which a surface has been continuously deformed to represent by its height the magnitude of the Franck–Condon factors as a function of v' and v''. We call this drawing, which resembles an aerial map of a geological formation, a "Condon diagram." Inspection of Fig. 8 reveals a set of mountain ranges which peak toward the (0, 0) origin. The broad front ridge has been called the principal Condon parabola,[17] although it is evident from the Condon diagram that (1) it is not parabolic in shape, (2) it is steeper on the left-hand side than on the right-hand side, and (3) it is not smooth, but has undulations of its own. The vibrational wavefunctions of the higher vibrational levels have broad maxima or minima near the classical turning points of the motion. Between these terminal loops there are smaller and narrower maxima and minima. The ridge of the front range of mountains shown in Fig. 8 arises from the constructive overlap of the terminal loop of one vibrational wavefunction with the terminal loop of the other. This corresponds

[35] When the radial Schrödinger equation is solved using the potentials given in Tables V and VI the calculated eigenvalues differ from the observed energy levels of the molecule by no more than 0.05 cm^{-1} on the average for either potential-energy function. As a further check on the accuracy of the vibrational wavefunctions calculated from the RKR potentials, the B_v value for each vibrational level is computed by evaluating the expectation value of $\langle 1/r^2\rangle$. The observed and calculated B_v values are found to differ by no more than 1×10^{-5} cm^{-1} for all the vibrational levels considered.

in the classical limit[36] to the molecule making a vertical transition upward or downward in the potential-energy diagram (Fig. 7).

Between the two arms of the so-called principal Condon parabola lies a complex series of rills which crisscross the enclosed area. These smaller hills and valleys result from the constructive and destructive interference between the intermediate maxima and minima of the vibrational wavefunctions in the overlap integral. These have been termed subsidiary parabolas,[17] although again the topography pictured in the Condon diagram belies such a simple description. Finally, to the far left of the Condon diagram we find a flat plain where the Franck–Condon factors all virtually vanish. A similar, but less pronounced, flat area lies on the near right of the Condon diagram. If this flatland were magnified many times a complicated undulatory structure would be seen superimposed on what appears to be an exponential decay toward zero.

In Figs. 2 and 3 we have shown the relative intensity pattern for fluorescence series originating from $v'=9$ and $v'=6$, respectively. If these intensities are compared with the Franck–Condon factors by checking in the appropriate column of Table VII, or alternatively, by following the appropriate horizontal line in Fig. 8, it is at once apparent that the observed and predicted intensity distributions are in good agreement. For example, in Fig. 2 the lines marked $(P, R0)$, $(P, R6)$, $(P, R8)$, $(P, R10)$, $(P, R13)$, $(P, R16)$, and $(P, R21)$ are the weakest members of the fluorescence progression. Table VII shows that these lines but no others have Franck–Condon factors less than 2×10^{-3}. In Fig. 3 the lines marked $(Q2)$, $(Q4)$, $(Q6)$, $(Q8)$, $(Q11)$, and $(Q17)$ are weakest. Again Table VII shows that these lines and no others have Franck–Condon factors less than 1×10^{-3}. The intensity pattern of each fluorescence series is quite distinctive, and there could be no confusion of one for the other. In this way, the spectroscopic analysis has been used to check our vibrational assignments. For the 19 fluorescence series (identified in Table II) that we were able to test in this manner, the observed intensity pattern is in good agreement with the calculated intensity pattern in every case.

It is hoped that this precise determination of the spectroscopic constants of Na_2 will demonstrate the usefulness of the laser-induced resonance fluorescence technique. In addition, this study makes Na_2 one of the best known simple molecules, and identification of the states involved in the various excitations by the argon-ion laser provides a basis for further study of this paradigm molecule by new spectroscopic methods. One example is provided in the following paper.

[36] See E. U. Condon, Am. J. Phys. **15**, 365 (1947).

ACKNOWLEDGMENTS

We are indebted to Dr. C. Keith McLane, who made available the comparator microdensitometer, and to William M. Welch, who aided us in the data reduction of the photographic plates. The close cooperation and good spirits of Dr. William R. Simmons and Dr. Donald A. Jennings, who shared the laser system with us, made our experimental efforts a great pleasure. We would also like to thank Dr. Harold S. Boyne, Chief of Division 271, National Bureau of Standards, and Dr. Lewis M. Branscomb, Chairman of the Joint Institute for Laboratory Astrophysics, whose support and encouragement made this collaborative venture possible.